Vrije Universiteit Brussel

VUB VRIJE
UNIVERSITEIT
BRUSSEL

Detailed numerical study of the peak shapes of neutral analytes injected at high solvent strength in short reversed-phase liquid chromatography columns and comparison with experimental observations
Pepermans, Vincent; Chapel, Soraya; Heinisch, Sabine; Desmet, Gert

Link to publication

1

2

3

4

Detailed numerical study of the peak shapes of neutral analytes injected at high solvent strength in short Reversed-Phase liquid chromatography columns and comparison with experimental observations

8

9

Vincent Pepermans[1], Soraya Chapel[2], Sabine Heinisch[2], Gert Desmet[1,*]

[1]*Department of Chemical Engineering, Vrije Universiteit Brussel, Brussels, Belgium*

[2] *Université de Lyon, Institut des Sciences Analytiques, UMR 5280, CNRS, 5 rue de la Doua, 69100, Villeurbanne, France*

[*]Corresponding author E-mail: gedesmet@vub.be

16
17
18
19
20
21
22
23
24
25
26
27
28
29
30
31
32
33
34
35
36
37
38
39

41

42

Abstract

We report on a numerical investigation of the different steps in the development of the spatial concentration profiles developing along the axis of a liquid chromatography column when injecting large relative volumes (>10 to 20% of column volume) of analytes dissolved in a high solvent strength solvent band as can be encountered in the second dimension (^{2}D) column of a 2D-LC system. More specifically, we made a detailed study of the different retention and the axial band broadening effects leading to the double-headed peak shapes or strongly fronting peaks that can be experimentally observed under certain conditions in 2D-LC. The establishment of these intricate peak profiles is discussed in all its fine, mechanistic details. The effect of the volume of the column, the volume and the shape of the sample band, the retention properties of the analyte and the band broadening experienced by the analytes and the sample solvent are investigated. A good agreement between the simulations and the experimental observations with caffeine and methylparaben injected in acetonitrile/water (ACN/H$_2$O) mobile phase with different injection volumes is obtained. Save the difference in dwell volume, key features of experimental and simulated chromatograms agree within a few %. The simulations are also validated against a number of simple mathematical rules of thumb that can be established to predict the occurrence of a breakthrough fraction and estimate the amount of breakthrough.

1. Introduction

As chromatography keeps being pushed by a demand for ever faster and more refined separations, more and more research efforts are devoted to two-dimensional LC (2D-LC), as this technique has the potential to produce peak capacities of several thousand in a practically affordable time [1-9] making the separation of difficult-to-resolve or complex mixtures easier and faster. During the transition of the sample from the first dimension ([1]D) to the second dimension ([2]D) column, some important problems such as dilution and solvent incompatibility effects arise when using a passive modulation method. In this approach, the [1]D-effluent is fractionated and directly injected into the [2]D, in most cases using a valve with multiple loops [10,11]. This often results in a loss of detector sensitivity and peak deformation in the [2]D [12-15]. To circumvent these problems, a lot of research efforts have been devoted to the active modulation between the two dimensions. One example is the use of trap columns [16-18] where the fractions of the effluent of the [1]D first get refocused, most often on a short column with a similar stationary phase as the [2]D column and are subsequently eluted using a solvent that is more compatible with the mobile phase used in the [2]D, potentially leading to an increase in sensitivity and solvent compatibility, and a lower injection volume. Active solvent modulation is another method that has been developed and investigated lately [19-21]. Here, by storing the [1]D effluent in a loop and splitting the [2]D mobile phase solvent, where one part goes through the loop and the other bypasses it, the fraction gets diluted before entering the [2]D column, which improves the solvent compatibility between the two dimensions. The idea to dilute the effluent of the [1]D column with a low elution strength liquid to induce appropriate focusing on the column's head has been first introduced by Oda et al. [22]. Other modulation methods are membrane assisted evaporation modulation [23], longitudinal thermal modulation [24], pulsed elution [18] and fractionated sampling and stacking [25].

To use these techniques more effectively and search for more universal methods of modulation, it is important to understand in detail what happens to an injected band inside the [2]D column when the [1]D-fractions are injected in this column. One of those factors is the solvent and injection solvent mismatch mentioned earlier, due to the fact that the injected species are dissolved in a solvent that is the effluent from the [1]D, which often has a higher solvent strength than the starting mobile phase in the [2]D. Another problem is that, given the column diameter ratio between the [2]D and [1]D (usually 1 to 2), the injection volumes in [2]D are often too large to maintain the maximal efficiency of the [2]D column. Generally, a 10% loss in efficiency is endured as soon as the variance of the injected band ($\sigma^2_{V,inj}$) makes up more than 10% of the expected column variance ($\sigma^2_{V,col}$), which is proportional to $(1+k)^2$, where k is the retention factor, and hence smallest for high elution strength mobile phases. The effect of the above phenomena on the shape of the peaks eluting off the [2]D column has already been thoroughly investigated theoretically and experimentally [15, 26-28]. Gritti [28] and Stoll et al. [15] also already demonstrated that the shape of the injection plug has a large effect on the eventual separation.

96 In the present study, we dig deeper into the processes leading to the obtained peak shapes by making a
97 fully detailed (numerical) study of how an injected band is transformed inside the column as (part of)
98 the analytes are first lagging behind the injection solvent band (because they are (slightly) retained by
99 the stationary phase) and are subsequently accelerated again when they are picked up by the mobile
100 phase gradient. To gain an insight in the axial, on-column evolution of the band, we use computer
101 simulations [29,30] based on the numerical solution of the generally accepted advection-dispersion mass
102 balance for chromatography [31]:

$$\frac{\partial C_t}{\partial t} = -u_0 \cdot \frac{\partial C_m}{\partial x} + D_{ax} \cdot \frac{\partial^2 C_m}{\partial x^2} \tag{1}$$

with $C_t = (1 + k) \cdot C_m$ (2)

and with $k = K \cdot \dfrac{V_s}{V_m}$ and $K = \dfrac{C_s}{C_m}$ (3)

103

104 wherein C_m and C_s are the analyte species concentration in resp. the mobile and stationary phase, u_0 is
105 the velocity of the mobile phase, D_{ax} is the axial dispersion coefficient, K is the partitioning coefficient,
106 t is the time, x is the position in the column and V_m and V_s are the volumes of the mobile and the
107 stationary phase respectively ($V_s/V_m = (1 - \varepsilon_T)/\varepsilon_T$) with $\varepsilon_T = 0.7$ in all simulations). The expression
108 in Eq. (1) is mathematically equivalent to the Craig-model approach developed by Rutan et al. [32], the
109 only difference is that, whereas in the Craig-model the spatial discretization scheme is fixed and 1st order
110 in nature, the more general approach in Eq. (1) allows for higher order accuracy schemes having a higher
111 numerical accuracy.

112 The D_{ax} describing the degree of band broadening in Eq. (1) is related to the u_0 and H via:

$$D_{ax} = \frac{u_0 H}{2} \tag{4}$$

113 Together with Eq. (1), we simultaneously also solve the advection-dispersion mass balance for the
114 fraction of organic modifier (ϕ). In analogy with Eq. (1), this can be written as:

$$\frac{\partial \phi}{\partial t} = -u_0 \frac{\partial \phi}{\partial x} + D_{ax} \frac{\partial^2 \phi}{\partial x^2} \tag{5}$$

115 Eqs. (1) and (5) were solved simultaneously using a 4th-order Runge-Kutta numerical integration scheme
116 to compute the evolution with time. During each step, the local ϕ-values are used to compute and update
117 the local value of the retention factor (k(x)), using either the LSS-model [33]:

$$k(x) = k_w \cdot e^{-S \cdot \phi(x)} \tag{6a}$$

118 Where k_w is the retention factor in 100% water, S is the solvent strength parameter and $\phi(x)$ is the local
119 value of the fraction of organic modifier, or the more elaborate Neue-Kuss model [34]:

4

$$k(x) = k_w(1 + S_2 \cdot \phi(x))^2 \cdot e^{-\frac{S_1 \phi(x)}{1 + S_2 \phi(x)}} \tag{6b}$$

120   Where S_1 is the slope for non-linear models and S_2 is the curvature coefficient.

121   As discussed previously, the program not only shows the peak profile as a function of time
122   (chromatogram) at the end of the column, but also provides a direct view on the evolution of the
123   concentration © with x, the axial location of the solute along the column. The effect of the retention
124   parameters (k_w, S or k_w, S_1 and S_2)) is thoroughly investigated, as well as the effect of the volume and
125   the shape of the injection plug and the effect of the column efficiency (via H and D_{ax}). Finally, the
126   program has been tested by comparing it with the experimentally observed breakthrough-curves at the
127   end of a short reverse phase liquid chromatography (RPLC) column under conditions mimicking the [2]D
128   of an on-line LC x LC separation. Upon simple email request, the authors offer access to the code to
129   Matlab® users.

130   Experimentally, the effect has been investigated for two different compounds, methylparaben and
131   caffeine, dissolved in a 50/50%v ACN/H_2O and subjected to a mobile phase gradient going from 1 to
132   45 (v%/v%) ACN. Characteristic for the elution of these compounds is that, under the selected
133   experimental injection conditions, they do not elute as a single peak but have a part eluting near the t_0-
134   time of the column (so-called breakthrough fraction), followed by a long tail connecting to a second
135   peak eluting near the expected retention time of the analyte (retained part of the peak). Similar peak
136   shapes have very recently also been reported by Weatherbee et al. [35], who found the exact peak shape
137   to be strongly depending on the shape of the injection profile.

138   **2 Materials and methods**

139   **2.1 Experimental set-up**

140   The experiments were performed on an ACQUITY UPLC I-Class instrument from Waters Corporation
141   (Milford, MA, USA) consisting of a binary solvent delivering pump (BSM), a sample manager with a
142   flow-through needle (SM-FTN) injector equipped with a 15 µL loop, a thermostated column oven, a
143   photodiode-array detector (PDA) with a 0.5 µL flow cell. An extension loop of 100 µL was added to the
144   injector. The measured dwell volume (V_D) and extra-column volume (V_{ext}) for this system were 210 µL
145   and 12 µL, respectively. The ACQUITY UPLC CSH C18 column (30 x 2.1 mm, 1.7 µm) was purchased
146   at Waters Corporation (Milford, MA, USA). Instrument control, data acquisition, and data handling were
147   performed by MassLynx v4.1 software (Waters Corporation).

148   **2.2 Solvents and samples**

149   Deionized water was produced using an Elga Purelab Classic UV purification system from Veolia water
150   STI (Décines-Charpieu, France). LC-MS grade acetonitrile (ACN), methylparaben and caffeine were
151   purchased from Sigma-Aldrich (Steinheim, Germany). LC-MS grade formic acid (FA) was purchased
152   from Fischer scientific (Illkirch, France).

2.3 Chromatographic conditions

The column temperature was set at 80 °C, the flow rate was 1.5 mL/min, and gradient elution was used with 0.1% formic acid in water as solvent A (pH = 2.7) and 0.1% formic acid in ACN as solvent B. The gradient profile went from 1-45% B in 0.54 min (normalized gradient slope (s) of 4%). The caffeine and the methylparaben were dissolved in a 50/50% (v/v) ACN/H2O mixture. The chromatograms were recorded at 254 nm for methylparaben and 270 nm for caffeine with an acquisition rate of 40 Hz.

2.4 Numerical methods

Eqs. (1) and (5) were solved with a 4th-order Runge-Kutta integration scheme [36] implemented in Matlab®. Before implementing the Runge-Kutta scheme, the spatial derivatives appearing on the right-hand side of Eqs. (1) and (5) were first discretized using the following scheme (with y either C or ϕ):

$$\frac{\partial y_i}{\partial x} = \frac{1}{\Delta x} \cdot \frac{1}{6}(y_{i-2} - 6y_{i-1} + 3y_i + 2y_{i+1}) \tag{7a}$$

$$\frac{\partial^2 y_i}{\partial x^2} = \frac{1}{\Delta x^2} \cdot \frac{1}{12}(-y_{i-2} + 16y_{i-1} - 30y_i + 16y_{i+1} - y_{i+2}) \tag{7b}$$

where Δx is the discretization step and i is the number of the cell in the column. Before and after the column (i.e., for x<0 and x>L=3 cm), resp. 1800 and 9200 extra computational cells were added. In these cells, the retention factor k was kept at k=0 to represent that the packed region only extended between x=0 and x=L=3 cm.

Zero-flux conditions ($\partial C/\partial x$=0 and $\partial \phi/\partial x$=0) were applied as the boundary condition at the first and last computational cells (resp. situated at x=-1.4 cm and x=10 cm). In addition, it was always verified the species concentration never became significant near the first and last computational cells, such that all possible end effects were avoided.

To implement the mobile phase gradient program, the ϕ-value at x=0 (ϕ_0) was subjected to the following condition:

$$\phi(x = 0, t) = \phi_0 \qquad \text{for } t \le t_D \tag{8a}$$

$$\phi(x = 0, t) = \phi_0 + \frac{\Delta\phi}{t_G}(t - t_0) \quad \text{for } t > t_D \tag{8b}$$

where t$_G$ is the gradient time and t$_0$ is the void time. As the initial condition for ϕ and C$_t$, an injection band containing the strong sample solvent (with ϕ=ϕ_S=0.5) and the analyte species (with C$_m$=1) was defined in the region x<0 with the downstream part of the band just touching x=0, i.e. the simulations started when the downstream end of the sample band just reached the column inlet.

To test the numerical accuracy of the model, a number of pure isocratic runs were made (see Fig. S-1 of the SM). These showed that the numerical procedure produces peak variances and hence plate heights

180 that are within 0.0000078% accuracy of the plate heights imposed in the model via the D_{ax}-coefficient

181 (see Fig. S-1a in the Supplementary material, SM). Retention times were found to be within 10^{-10} %

182 accuracy of the theoretically expected value.

183 In case of the simplified rectangular injections (used in the first part of the study to obtain the purest

184 possible insight in the peak shapes without the complication of the effect of the complex shape of the

185 injection band), the injection band was defined as a rectangle with given width, flanked by two semi-

186 Gauss curves with a standard deviation (σ_x) = 0.012 cm. These two Gaussian flanks were added to make

187 the injection profile more realistic, but especially also to avoid the numerical instabilities one can expect

188 from a perfectly vertical side-walls of a rectangle (concentration gradient= infinite). Given the strong

189 sensitivity of the profiles on the exact shape of the injection band, more realistic injection band shapes

190 were considered in the second part of the study. These were shaped using an expression developed by

191 Gritti [28]:

$$C(0,t) = \frac{C_0}{1 + \exp\left(-\frac{t - t_{dwell} + \frac{V_p}{2F_v}}{\alpha_1}\right)} \cdot \left[1 - \frac{1}{1 + \exp\left(-\frac{t - t_{dwell} + \frac{V_p}{2F_v}}{\alpha_2}\right)}\right] \tag{9}$$

192 Wherein C_0 is the concentration of the initial peak (can also be the fraction of organic solvent), t is the

193 time the measurement is running, t_{dwell} is the dwell time in front of the column, V_p is the injected volume,

194 F_v is the flow rate, and α_1 and α_2 are two fitting parameters.

195 This equation was first implemented in MS Excel® and subsequently incorporated into the Matlab©

196 program.

197

3. Results

199 Before proceeding, it is important to note that the injected species band and the profile of the fraction ϕ

200 of organic modifier in the sample solvent always have the same shape when they enter the column (see

201 e.g., profile 1 in Figs. 1b,e) in any considered case. In the regions before and after the injection band, ϕ

202 is equal to the fraction of modifier (ϕ_0) in the dwell volume of the gradient (equal to ϕ_0=0.01 in all

203 cases). The fraction of modifier is highest ($\phi=\phi_S$) in the parts of the injected band that enter the column

204 undiluted. In all considered cases, ϕ_S=0.5. Another important remark is that, while the conservation of

205 mass is expressed via the total peak concentration (C_t) (cf. Eq. 2), the response as measured by the

206 detector is exclusively determined by the concentration in the mobile phase (C_m), given the absence of

207 a stationary phase in the detector.

208 Fig. 1 describes in full detail how the simulation of the evolution of the concentration in time and space
209 can be used to understand how a given injected peak shape and volume can lead to a given chromatogram
210 recorded at the end of the column. For the sake of simplicity, a simple rectangular injection profile with
211 smoothened flanks (cf. Section 2.4) has been considered. In later figures, notably in Figs. 6-8, more
212 realistic injection profiles are considered by applying Eq. (9). Fig. 1a is the response in time as observed
213 at x=L, i.e., at the end of a 3 cm long column (L). Figs. 1b-c represent how the same injected band is
214 distributed in space at different time intervals (note that the left hand side of the peak in the time domain
215 corresponds to the right hand side of the peak in the space domain and vice versa). The numbers used to
216 identify the timing of the different profiles in Figs. 1b-c are also copied onto Fig. 1a, allowing to
217 reconstruct the observed concentration response at the detector line (cf. dashed vertical line) from the
218 temporal evolution of the band profiles in space shown in Figs. 1b-c. Profile (1) shows the shape of the
219 modeled analyte band peak just prior to arriving at the column's head.

220 Essential to understand the profiles in Figs. 1b-c is that, when a broad analyte band moves through the
221 column, the species that are initially contained in the high-solvent strength solvent band can leave this
222 band by means of two processes: 1) by means of their retention, which makes them move with a lower
223 velocity than the u_0-velocity with which the injection solvent band moves through the column and 2) by
224 means of dispersion across the band flanks.

225 Considering the first process, which is by far much more important than the second, the slower migration
226 velocity of the analytes obviously implies the analytes stay behind with respect to the sample band and
227 hence "leave" the band through the upstream flank of the injection solvent band (Fig. 2a). The magnitude
228 of this effect obviously depends strongly on the retention experienced by the analytes when dissolved in
229 the injection solvent (k_s=0.1685 in the present example). Once out of the injection solvent band, the
230 species inevitably enter a low-solvent strength zone where they concentrate in the stationary phase.
231 Considering the 2nd process, Fig. 2b shows that, whereas the dispersion process itself is substantially
232 symmetrical (i.e., has an equal strength in the upstream and downstream direction), the effect on the
233 peak profile can be expected to be asymmetric. Species leaving the band through its downstream flank
234 by means of dispersion (double-headed dispersion arrow I) are suddenly strongly retained and drastically
235 slow down. However, they are immediately caught up again by the high-solvent band following behind
236 and moving with the u_0-velocity (cf. large single-headed arrow). This creates a self-sharpening effect,
237 which helps maintaining a steep species profile at the upstream flank of the band. On the other hand,
238 species leaving the band through its upstream flank (dispersion arrow II), and thus entering a high
239 retention zone, cannot benefit from a similar self-sharpening effect as there is no front of strong solvent
240 following. As a consequence, these analytes stay behind permanently. In summary, both processes hence
241 lead to situation where the band can be expected to "leak" species through its upstream flank and thus
242 deposits a trail of retained species along the column axis.

243 Returning now to the spatial C_m-concentration profiles in Fig. 1b, it can be readily observed the species

244 band continuously narrows in width as the analyte species gradually leave the sample solvent band

245 through its upstream flank because of the slower migration velocity of the analytes (migrating with

246 velocity $u_0/(1+k_s)$ with $k_s=0.1685$ in the sample solvent) compared to that of the sample solvent

247 (migrating with velocity u_0). The latter basically retains its original shape (save for the gradual

248 broadening of its side fronts because of the column band broadening) throughout its entire passage

249 through the column (see Fig. 1e which has been put just underneath Fig. 1b for an easy comparison of

250 the corresponding profiles). Comparing the C_m-profiles in Fig. 1b with the ϕ-profiles in Fig. 1e in more

251 detail, we see that the upstream flank of the analyte band and that of the sample solvent band coincide,

252 while the downstream flank of the analyte band stays behind with respect of that of the sample solvent

253 band, as a reflection of the lower migration velocity of the former. When the analyte band has become

254 sufficiently narrow to have its upstream and downstream flank meeting, the further loss of analyte

255 species not only leads to a further narrowing of the band, but also to a decrease in peak height (cf. profiles

256 4,5,6 in Fig. 1b). Note that the fact that the decrease in height between profiles 5 and 6 is smaller than

257 that between profiles 4 and 5 is due to the absence of a stationary phase beyond the $x=0.03$ m-point.

258 Zooming-in on the bottom part of Fig. 1b (see expanded view added to Fig. 1a), it can be noted that the

259 analytes that left the sample band form a trail of analyte species running from the column's head all the

260 way up to the upstream flank of the sample solvent band.

261 Making now the link between the spatial profiles in Fig. 1b with the temporal response curve in Fig. 1a

262 by linking the profile numbers, we see that the fraction of analytes that remained into the sample solvent

263 band till the end of the column is recorded at the detector as the breakthrough part of the peak (indicated

264 with letter A in Fig. 1a), with the rise and fall of this part of the breakthrough curve essentially occurring

265 during the moments between profiles 4 (just before onset of breakthrough peak) and 6 (end of

266 breakthrough peak). The breakthrough reaches its maximum close the moment relating to profile nr. 5,

267 corresponding to the t_0-time of the column. After the passage of this breakthrough part, the concentration

268 of eluting analytes does not return to zero but stays at a small, yet clearly non-zero value because of the

269 continuous (albeit slow) elution of the analytes species that dropped out of the sample solvent band.

270 While the peak profiles in Fig.1 b appear to lose mass (cf. reducing peak area), it is very important to

271 note these profiles only represent the concentration C_m in the mobile phase, while the concentration C_s

272 in the stationary phase is in fact K times (K=phase equilibrium constant) higher. Fig. 1d shows the

273 stationary phase concentration C_s corresponding to the profiles shown in Fig. 1b. Near their upstream

274 end, these profiles display a very sharp peak, rapidly transiting into a substantially flat part. As the

275 sample band progresses through the column, this flat part gradually expands in width until the end of

276 the column at $x=3$ cm is reached. The C_s-value in this flat part is dictated by the fact that the analytes in

277 the sample solvent band have a concentration $C_m=1$. Since the retention factor k_s in the sample solvent

278 (ϕ_S=0.50) in the present example is equal to k_s=0.1685, the corresponding particle-zone equilibrium
279 constant K is equal to K=$k_0 V_m/V_s$= k(1-ε_T)/ε_T = 0.3932 (assuming ε_T=0.7). We can hence expect a C_s-
280 concentration C_s=K·C_m=0.3932·1=0.3932 wherever C_m=1 concentration in the injection band and this
281 is indeed the level at which the flat part of the C_s-profiles is situated. Upstream of the sample solvent
282 band, the C_s-concentration remains at this level, as there is no driving force to deplete the stationary
283 phase. What does change is the C_m-concentration, which, given the retention factor k_0 in the weak solvent
284 (ϕ_0=0.01) preceding and proceeding the sample solvent band is equal to k_0=17.75, can be expected to
285 be K=$k_0 V_m/V_s$= k(1-ε_T)/ε_T = 41.42 times lower than the C_s-concentration. And as can be noted from the
286 inset of Fig. 1b this is indeed the case. Turning now to the sharp peak at the upstream end of the C_s-
287 profile, a detailed analysis of the profiles (data not shown) shows this is created when the upstream tail
288 of the band enters the column. As ϕ rapidly drops from ϕ=0.5 to 0.01 in this tail part, the analyte species
289 entering the column in this tail end slow down much more abruptly than their counterparts that entered
290 the column earlier. This leads to a local accumulation of species, which is further enhanced by the fact
291 that the analytes following behind do not experience this deceleration effect and keep on entering the
292 column with an unretained velocity (no stationary phase before x=0). The subsequent profiles 2-6 in Fig.
293 1b and 1d show how this accumulated sharp peak slowly moves (in fact it does so with a velocity
294 u_0/(1+17.55) given the fact that k=17.75 in the ϕ=0.01 mobile phase in the present example.

295 At later stages of the elution process (cf. Figs. 1c and 1f), i.e., when the gradient program has increased
296 the fraction of organic modifier to a sufficiently high level at the inlet of the column, the increase in
297 solvent strength gradually releases the retained species that are distributed over the entire column length.
298 As these species gradually dissolve again into the mobile phase, their velocity increases. And as the
299 fraction ϕ of organic modifier is higher on the left-hand side than on the right-hand side, the upstream
300 situated species migrate faster than the downstream moving species, and a self-sharpening effect again
301 establishes. As a consequence, the upstream side of the species band rapidly grows in height ('scooping-
302 up effect"). Obviously, this self-sharpening effect is highest at the upstream end of the band, as this is
303 where species pick up their highest velocity, but the effect nevertheless occurs over the entire length of
304 the column, thus giving rise to an increase of the C_m-concentration over the entire extent of the species
305 profile.

306 Subsequently focusing on the value of C_m along the vertical dashed line at x = 0.03 cm (detector line) in
307 Fig. 1c, it can be understood how the species concentration gradually increases at the detector when the
308 spatial profiles 7-11 subsequently hit the detector line. The response at the detector obviously reaches
309 its maximum shortly after the moment at which profile nr. 10 is established. Subsequently, the
310 concentration at the detector rapidly drops to zero (cf. profile 11). This second peak top (cf. "B" in Fig.
311 1a) is further referred to as the retained peak, as it elutes near the time of elution expected based on the
312 gradient program and the retention parameters of the analyte.

313 In summary, the entire process described above leads to a double headed-peak shape, with one maximum

314 near the breakthrough peak and one maximum near the retained peak position (=position where analytes

315 are expected to elute when the volume is sufficiently small). In between, the signal does not return to

316 the baseline, as a continuous stream of analyte species that "leaked" out of the sample solvent band close

317 to the end of the column keeps on eluting off the column, albeit at a low concentration and a low velocity

318 ($u=u_0/(1+17.75)$). For the sake of comparison, Fig. S2 in the SM shows that when the sample is dissolved

319 in the solvent marking the onset of the gradient a single neat peak is obtained is in this case the analytes

320 are so strongly retained they immediately leave the sample band when entering the column.

321 Fig. 3 shows how strongly the profile recorded at the detector response depends on the retention

322 parameters of the solute. Adopting the Neue-Kuss model, where the retention is described by k_w

323 (=retention factor in 100% water), S_1 (=solvent strength parameter) and S_2 (describes the curvature of

324 the model) via $k=k_w(1+S_2\phi)^2 \cdot e^{-S_1\phi/(1+S_2\phi)}$, Fig. 3a shows that the broad, double-headed response profile

325 similar to the one encountered in Fig. 1 is typically observed when k_w is sufficiently low. For larger k_w,

326 the chromatogram narrows and ultimately, when k_w is sufficiently large, displays the shape and elution

327 time of a normally retained peak. This can be understood from the fact that, the lower k_w, the lower the

328 actual retention factor k_s experienced by the species in the solvent sample band, and hence the further

329 they can travel without leaving this band. If k_w is sufficiently low and when the volume of the band is

330 large enough, some of the sample species will still reside in the injection solvent band when this reaches

331 the detector and are hence detected as a "breakthrough" part. In the extreme limit ($k_w=0$), all species

332 reach the detector together with the injection solvent band and there is only a breakthrough peak. In the

333 other limit ($k_w=+\infty$), all species are so strongly retained at the inlet of the column that they immediately

334 leave the injection solvent band, in which case there is no breakthrough part of the peak, and all species

335 now elute within the retained part, reaching the detector by means of the gradient. The profile for the

336 highest k_w in Fig. 3a approaches this situation. For the intermediate k_w-values, it is obvious to observe

337 some mixed-mode behavior. The effect of S_1 (Fig. 3b) can be rationalized following the same reasoning

338 as above. Since all cases have the same k_w, the highest S_1-values now correspond to the case producing

339 the lowest retention factor k_s experienced in the sample solvent, thus transporting the largest fraction of

340 species along with the sample band through the column and creating the largest breakthrough curve

341 (grey curve). The lowest S_1-values obviously leads to the highest k_s, such that the analyte species already

342 leave the sample band at the column's head, and will therefore reach the detector by virtue of the mobile

343 phase gradient as a normal chromatographic peak at the retention time predicted by the Neue-Kuss

344 model (red curve).

345 Fig. 4 investigates the effect of the column's band broadening on the concentration profiles recorded by

346 the detector (only zoom-ins of the breakthrough-fraction and the retained peak fraction are shown for

347 the sake of compactness). All represented cases relate to the same rectangular injection band shape, and

348 are compared to a base case (grey curve) where the band broadening (axial dispersion) for both the

349   sample solvent and the analyte is the same and represented by a value $D_{ax} = 3.86 \cdot 10^{-8}$ m^2/s in Eq. (1).

350   Keeping the axial dispersion coefficient of the analyte ($D_{ax,an}$) constant and gradually increasing that of

351   the solvent ($D_{ax,solv}$), which corresponds to the practically most relevant case, Figs. 4a shows that a larger

352    $D_{ax,solv}$ tends to lower the breakthrough fraction while increasing (albeit it more moderately) the retained

353   peak fraction. This can be understood as follows. The higher $D_{ax,solv}$, the faster the sample solvent will

354   mix with the surrounding low ϕ-mobile phase. This leads to a reduction of the overall ϕ in the band

355   (especially near its ends), giving rise to larger fractions of the sample band that are subjected to a

356   retention factor $> k_s$, such that more species tend to leave the sample solvent and hence no longer reach

357   the detector together with the breakthrough fraction in the sample solvent band. As more analyte species

358   drop out, it is also physically straightforward that more species only pick up speed again when they are

359   caught up by the gradient and hence reach the detector with the retained peak fraction. Increasing $D_{ax,an}$,

360   while keeping $D_{ax,solv}$ constant, the effect is smaller (Fig. 4b), basically boiling down to the regular effect

361   an increased band broadening can be expected to have on a chromatographic peak: the higher the axial

362   dispersion, the broader the peak. The increasing asymmetry and shift of the peak apex to earlier elution

363   times of the breakthrough peak that can be observed with increasing $D_{ax,an}$ in Fig. 4b can be understood

364   as follows (see also Fig. S-3 in the Supplementary material (SM) for a detailed study of the on-column

365   C_m- and the ϕ-profiles in case of the lowest and the highest $D_{ax,an}$): while the downstream flank

366   (=fronting end) of the analyte band can display its normal, unrestricted band broadening behavior as it

367   is immersed in the high $\phi = \phi_S$-sample solvent prevailing to its right, the upstream flank C_m-profile of

368   the analyte band inevitably (because of the thermodynamic phase equilibrium that needs to be respected)

369   coincides with the (steep) upstream flank of the sample solvent (see dashed vertical lines added to Fig.

370   S-3). As a consequence, the drop in C_m observed at the upstream flank is not due to the band broadening

371   but is dictated by the drop in ϕ along the upstream flank of the sample solvent band. This drop chases

372   the analytes out of the mobile phase into the stationary phase. Since $D_{ax,solv}$ is kept constant in all elution

373   profiles shown in Fig. 4b (and equal to the smallest considered $D_{ax,an}$), the discrepancy between the

374   unrestricted band broadening at the downstream flank of the analyte band and the drop in concentration

375   along the steep ϕ-curve at its upstream flank increases with increasing $D_{ax,an}$, hence the increasing

376   asymmetry of the breakthrough peaks in the profiles obtained with increasing $D_{ax,an}$.

377   Increasing $D_{ax,an}$ and $D_{ax,solv}$ simultaneously (Fig. 4c), clearly a combination of both aforementioned

378   effects is obtained, in agreement with one's physical expectations.

379   Obviously, the shape of the recorded elution profiles also depends strongly upon the injection volume

380   (Fig. 5). The larger the volume of the sample solvent band, the larger the relative fraction of species in

381   the breakthrough peak. This is due to the fact that, the wider the injection solvent band, the longer it

382   takes the analyte to escape from the injection solvent, as it takes ever longer for the analytes entering the

383   column near the downstream flank of the sample band (point A in Fig. 2a) to be overtaken by the

384   upstream front of the sample band (point B in Fig. 2a). Under the conditions assumed in Fig. 5, the 50,

385   25, 15 and 12 μL injections are apparently wide enough to transport a fraction of the analytes through

386   the column without having "leaked out" of the injection solvent band, thus displaying a breakthrough

387   part. For the 50 μL injection, the breakthrough fraction is very large, while this fraction is only minimal

388   for the 12 μL injection (cf. small bump around t=0.065 min in Fig. 5c). When the injection solvent band

389   is small enough, all injected species leave the sample band before this reaches the end of the column,

390   hence the absence of a breakthrough part in the elution profile for injection volumes 1, 5 and 10 μL.

391   While the injection volumes ≥ 15 μL are large enough to spread the retained analyte species more or

392   less uniformly across the entire column length during the passage of the injection solvent band (cf.

393   situation for profiles 4, 5, 6 in Figs. 1b and 1e), the injection solvent bands with volumes < 12 μL "lose"

394   all the analyte species they initially contained before reaching the end of the column. The latter can be

395   noted from the fact that the profiles corresponding to these volumes only start to rise well after the t_0-

396   time of the column, i.e., well after the injection solvent band has left the column. This can be understood

397   from the fact that, the smaller the sample band, the earlier on in the column all analytes will have left

398   the injection solvent band. As a consequence, these species will not have travelled very far into the

399   column at the moment at which they are caught up by the gradient and will hence reach the detector

400   later. This explains why the rise in concentration observed in Figs. 5b and 5d (=zoom-in of b) starts ever

401   later when the injection volume decreases (a detailed analysis of the establishment of the black-coloured

402   profile in Fig. 5d is shown in Fig. S-4 of the SM wherein profile 1 is the axial C_m-profile at the moment

403   of elution of the sample solvent band). Eventually, the 1 μL injection is so small that all species already

404   dropped out of the injection solvent band in the very first fractions of the column. Consequently, they

405   all basically start at the same starting point when they are picked up by the gradient and hence reach the

406   detector as a "normal" Gaussian peak without any fronting.

407   In fact, the conditions for the occurrence of a breakthrough peak can, with reference to Fig. 2a, easily be

408   determined as follows, at least when neglecting the secondary effects originating from the band

409   broadening process (most prominent for small injection volumes). Consider an analyte entering the

410   column at the most downstream end of the sample band (point A). This will move with a velocity

411    $u_A=u_0/(1+k_s)$ and will, since $u_A<u_0$, therefore eventually be caught up by the upstream flank of the

412   injection solvent band which travels at a velocity u_0. Denoting the time at which point B catches up with

413   point A is time t^*, we can now express that this is the moment at which both points have reached the

414   same position $x=x^*$ in the column:

415                                $x^*=u_0 \cdot t^*=w_{p,col}+ u_A \cdot t^*$ (10)

416   wherein $w_{p,col}$ is the width of the band when present in the column and in contact with a stationary phase

417   with retention factor k_s.

418   Replacing u_A by its relation to u_0 in Eq. (10), it is found that:

$$420 \quad t^* = \frac{w_{p,col}}{u_0} \cdot \frac{1 + k_s}{k_s} \tag{11}$$

419

420   Since the analytes at position A will be the last species leaving the injection solvent band (cf. Fig. 2a),

421   we can express that there will always be a fraction of the analytes traveling through the column with the

422   injection solvent band as long as the time t^* is not reached within the residence time of the sample solvent

423   band. Translating this into distance, we can state that the response at the detector will display a

424   breakthrough fraction when the catching up point x^* is situated after the detector, or $x^* > L$. Hence

425   combining Eqs. (10) and (11), we find:

$$426 \quad x^* = u_0 \cdot t^* = w_{p,col} \frac{1 + k_s}{k_s} > L \tag{12}$$

427   Translating the on-column peak width into the on-column peak volume ($V_{p,col}$, assuming for simplicity

428   a rectangular band shape) and comparing it to the injected peak volume ($V_{p,inj}$) measured before entering

429   the column, considering that $V_{p,col} = A \cdot \varepsilon_T \cdot w_{p,col} = V_{p,inj}/(1+k_s)$, while the column void volume ($V_{0,col}$) can

430   be written as $V_{0,col} = A \cdot \varepsilon_T \cdot L$, the condition to have a detector response with a breakthrough part expressed

431   by Eq. (12) can simply be rewritten as:

$$432 \quad V_{p,inj} > V_{0,col} \cdot k_s \tag{13}$$

433   In case of a Gaussian-shaped band with $w_{p,col} = 4\sigma$, the right-hand-side of Eq. (13) needs to be multiplied

434   with a factor 0.63 (i.e., $\sqrt{2\pi}/4$).

435   Eq. (13) implies that, for example, for a column with volume 100 μL and an analyte displaying a

436   retention factor of $k_s = 0.5$ in the injection solvent, a breakthrough will occur for injection volumes

437   exceeding 50 μL. When $k_s = 0.1$, breakthrough will already occur for injection volumes in excess of

438    $V_{p,inj} = 10$ μL. The simulations in Fig. 5 have been carried out for a column volume of 72.7 μL, and with

439    $k_s = 0.1685$. Applying Eq. (13) then predicts the critical injection volume lies around 12 μL (12.25 μL to

440   be precise). The fact that the 12 μL-case in Fig. 5 leads to a breakthrough that is barely significant (small

441   bump around t_0-time in Fig. 5c) hence shows the simulations and the simple model developed above are

442   in excellent agreement.

443   Using a similar calculation, it can be shown that the condition for which all sample species leave the

444   sample band "early", defined here as having left the band within a distance not exceeding the initial

445   width of the sample solvent band w_{solv} (with $w_{solv} = V_{inj}/\varepsilon_T \cdot A = w_p^*(1+k_s)$ wherein w_p^* is the initial width

446   of the species band), is simply given by:

$$447 \quad k_s \geq 1 \tag{14}$$

448   To prove Eq. (14) it suffices to replace L by w_p on the right-hand side of Eq. (12).

449 Similarly, it can be demonstrated (replacing L by 2L on the right-hand side of Eq. (12)) that the condition

450 leading to a breakthrough peak bringing half of the species to the detector while the other half of the

451 band then reaches the detector at the expected retention time is given by:

452
$$V_{p,inj} = 2.V_{0,col} \cdot k_s \qquad (15)$$

453 Eq. (15) predicts this condition corresponds, for the presently considered case with $V_{0,col}$=72.7 µL and

454 with k_s=0.1685 to an injection volume of $V_{p,inj}$=24.5 µL. It has been verified by calculating the area

455 under the breakthrough part of the 25 µL injection (orange-coloured curve) in Fig. 5 that this part of the

456 curve indeed carries about 50% of the total injected mass (53% to be precise in represented case).

457 An important remark to be made concerning Fig. 5 is that, while this figure illustrates the effect of the

458 injection volume $V_{p,inj}$ on the peak shape, the ultimate parameter controlling the detector response is in

459 fact the relative peak volume, i.e. $V_{p,inj}/V_{0,col}$. This is shown in Fig. S-5 of the SM where the response to

460 a 15 µL injection in a column with a 72.7 µL void volume overlaps fairly well with the response to a 30

461 µL injection in a column with a 145.4 µL void volume (at least provided the t_G and dwell time is doubled

462 as well). The importance of the relative parameter $V_{p,inj}/V_{0,col}$ can also be inferred from the fact that,

463 when dividing both sides of Eqs. (13) and (15) by $V_{0,col}$, expressions depending only on $V_{p,inj}/V_{0,col}$ and

464 k_s are obtained. The small deviation between the two profiles in Fig. S-5 is due to secondary effects of

465 band broadening which are not included in the simplified analysis in Eqs. (10)-(15).

466 Fig. 6 shows that not only the volume but also the actual shape of the injected band has an important

467 effect on the resulting elution profile, with the shape of the tail (Fig. 6a) being significantly more

468 important than the shape of the front (Fig. 6b). The explanation for this asymmetric behavior is the same

469 as for the asymmetry discussed in Fig. 2b. Considering that the shape of the band flanks determines the

470 amount of species that are present in a low ϕ-mobile phase and are hence much more strongly retained

471 than the species in the center of the band where $\phi = \phi_S$, it is physically straightforward to expect that

472 the initial shape of the downstream flank will always be largely wiped out by the fact that the retained

473 species in this flank are always caught up and thus accelerated again by the high ϕ-region in the center

474 of the sample band, while this self-sharpening catching-up effect does not occur at the upstream flank

475 of the sample band. This implies the initial shape of the upstream flank is not rectified (even more, it

476 will only spread out further by the column's dispersion) and hence directly determines the amount of

477 analyte species staying behind the sample solvent band at each position along the entire column length.

478 Obviously, this has a strong effect on the recorded elution profile for the short column (typical for 2D-

479 LC) considered here. For example, Fig. 6a shows that, whereas a steep upstream flank leads to a narrow

480 and high breakthrough peak, this breakthrough part no longer appears in case of a strongly tailed

481 injection band (which is in fact a shape that is very relevant in practice [27]). This can be understood as

482 follows: the more rectangular in shape, the larger the fraction of injected species that remain dissolved

483 in the mobile phase with the highest ϕ at any time during the band's migration, and hence also the higher

484   the fraction that can be transported through the column with the injection solvent peak. The wider the

485   tail, the lower the average ϕ-value experienced by the migrating analytes and hence the more easily they

486   leave the sample solvent band. When this average ϕ falls below a certain threshold, all analytes leave

487   the injection solvent band by retention before the sample band reaches the end of the column, as happens

488   in case of the orange curve. In this case, all analytes have to wait for the gradient to pick up speed and

489   hence reach the detector all around the normal elution time. This explains the order of the retained peak

490   apexes just before t=0.4 min.

491   As explained above, the effect of the shape of the downstream flank is much smaller (Fig. 6b). The

492   retained peak part of the elution profile is even completely insensitive to this shape. The only difference

493   is notable for the breakthrough peak, which seems to be engaged in a "communicating vessel" exchange

494   with a small bump eluting shortly after the breakthrough peak. The fact that it is precisely the initial

495   parts of the elution profile which are affected by the initial band shape is physically expected, as the

496   species present in these early eluting fractions must have reached the detector while residing in the

497   injected sample band, and are therefore most affected by the shape of the latter. The establishment of

498   the small bump just before t=0.25 min can be best understood from the subsequent axial distribution

499   profiles recorded during the simulation (Fig. S-6). These show that, in this particular case, the last

500   fraction of analytes leaves the sample solvent band just before the end of the column. In addition, the

501   rate with which the analytes leave this band strongly increases just when the last fraction of analytes

502   leaves the sample solvent band, as the average ϕ-value experienced by the remaining analytes rapidly

503   drops in these last moments (cf. average ϕ-value for situation in Figs. S-6c-d in the SM). This

504   accelerated drop-out rate gives rise to a local maximum in the species concentration in the stationary

505   phase (C_s), where the majority of the species are stored once they entered the low solvent-strength

506   solvent (ϕ_0). The magnitude of this local maximum depends on the exact shape of the concentration

507   gradients, such that it is more pronounced in some cases than in others. When this local maximum in the

508   C_s-profile is formed far away from the column end, i.e., when all analytes leave the sample band

509   sufficiently far away from the column's end, the presence of this local maximum is already eroded by

510   the ongoing dispersion processes by the time this fraction of the analytes reaches the detector. However,

511   when the local maximum is formed close to the column's end, as is the case for the situation in Fig. 6b,

512   the local maximum is maintained in the C_m-concentration reaching the detector.

513   Fig. 7 and 8 investigate how well the simulations can represent the experimental data, taking caffeine

514   (Fig. 7) and methylparaben (Fig. 8) as the test analytes and using the retention parameters (cf. k_w and S_i-

515   values in Eq. 6) as measured via independent experiments. Important to note here is that the exact shape

516   of the injected bands in the experimental part of this study is unknown to us and that the shape used here

517   has been obtained by trying different variants of the peak shape represented by Eq. (9) and selecting the

518   one providing the best agreement (see Fig. S-7a in SM for exact shape and degree of tailing and fronting

519   of the considered injection profile). Whereas this profile has been obtained using Eq. (9), it should be

520 remarked it is very similar to the profiles observed in [35] (appears backwards, because Figure S-7 is

521 shown on the distance axis, and the profiles shown in [35] are shown on a time axis).

522 As can be noted, the qualitative agreement is very good, especially in terms of the effect of the injection

523 volume. The small deviations can be attributed to differences in extra-column band broadening (only

524 simulated here by adding a perfect mixer with volume= 6 μL= volume detector + post-column capillary),

525 small uncertainties on the adopted relation between k and ϕ as well as the aforementioned uncertainty

526 on the exact injection band shape. The slightly larger breakthrough times in the experiments compared

527 to the simulations are probably due to the fact that the acetonitrile in the sample solvent band is also

528 slightly retained as well [37]. The largest deviation between theory and experiment is observed in the

529 initial part of the 25 μL-volume injection for methylparaben (blue curve in Fig. 8d). The deviation

530 observed in this initial part is most probably due to the uncertainty on the exact shape of the injection

531 band shape and the value of the retention parameters of the analyte, as the initial part of the response is

532 most sensitive to the band shape and the retention parameters and we don't have an exact knowledge of

533 them. The peculiar shape displayed by the blue curve in Fig. 8d between 0.2 and 0.3 min is caused by

534 the same phenomena as already described via Fig. S-4 and S-6 of the SM. A detailed analysis of the

535 present case is shown in Fig. S-7 of the SM.

536 **4. Conclusions**

537 Numerical simulations of the in-column axial distribution and migration of analyte species obtained by

538 solving the general advection-dispersion mass balance for the analytes and the organic modifier used in

539 the mobile phase and the sample solvent allow to understand the complex peak shapes that can be

540 obtained when injecting large peak volumes (i.e., large with respect to the column volume) dissolved in

541 a strong solvent, as can be the case in the ^{2}D in contemporary 2D-LC.

542 The axial concentration profiles produced by the simulations show how the elution under this condition

543 basically occurs in two steps. In the first step, analyte species are transported along (part of) the column

544 with the sample solvent band (unretained and hence moving at u=u$_0$) leading to two fractions: 1) a

545 fraction that reaches the detector together with the sample solvent (fraction only if Eq. (13) is satisfied)

546 and 2) a fraction leaving the sample solvent band through its upstream flank and thus being spread out

547 along (part of) the column length. In a second step, the species from fraction 2), being concentrated in

548 the stationary phase and hence moving very slowly as soon as they dropped out of the sample band and

549 entered the low modifier mobile phase following behind the sample solvent band, are eventually

550 "scooped up" by the gradient which accelerates them towards the detector where they are recorded as a

551 retained peak. The latter originates from the self-sharpening effect (band compression) of the gradient

552 profile on the spread-out species that left the sample solvent band. Depending across what fraction of

553 the column length the analyte species are spread out (in turn depending on the injection volume and the

554 retention factor in the sample solvent k$_s$), this retained peak can be very broad and fronted (large part of

555 column length covered with analyte species when the onset of the gradient reaches the column) or have

556 a "normal" retained peak shape (analytes already left the sample band shortly after entering the column).

557 When the analyte species are distributed along the entire column length (i.e., when Eq. (13) is satisfied),

558 the peak signal does not return to zero between the breakthrough and the retained peak part, thus forming

559 an uninterrupted, double-headed peak.

560 Given the short length of the investigated column, the eventually recorded peak shape not only depends

561 strongly on the volume but also on the exact shape of the injected sample band, as was also observed by

562 Weatherbee et al. [35]. The degree of band broadening experienced by the analytes and the sample

563 solvent (which are in general different from each other) contributes significantly to the eventual peak

564 shape as well.

565 Whereas the simulation model is based on first-principles physical relations, with all its parameters fixed

566 by taking the values measured in independent experiments and whereas the use of an idealized injection

567 (rectangular) profile was already sufficient to predict the main characteristics of the observed

568 breakthrough (% of breakthrough, general shape of the profile, elution times of breakthrough and

569 retained fraction), a one-on-one agreement with all the fine details of the experimental response curve

570 requires a close representation of the injection profile. As the latter information was experimentally

571 inaccessible in the present study (see ref. [38] for a possible way to measure the injection profile), this

572 had to be done by tuning the α_1- and α_2-parameters in the literature expression in Eq. (9). As all the

573 other model parameters were obtained from independent experiments, the good agreement between the

574 simulation results and the experiments can hence be used to conclude there is a sound theoretical

575 explanation for the experimental observations.

576 Finally, it is important to remark that the observed effects of prak splitting are difficult to avoid in the

577 context of 2D-LC given the many constraints that need to be satisfied when optimizing 2D-LC

578 separations. The most effective way to avoid them would be to use on-line dilution, flow splitting or trap

579 columns. Most of these solutions however lead to a loss of sensitivity and require a change in set-up.

580

584

585

586

587   **References**

588   [1] D.R. Stoll, X. Li, X. Wang, P.W. Carr, S.E.G. Porter, S.C.Rutan, Fast, comprehensive two-
589   dimensional liquid chromatography, J. of Chromatogr. A 1168(1-2) (2007) 3-43.
590   DOI: 10.1016/j.chroma.2007.08.054
591

592   [2] M. Sarrut, A. D'Attoma, S. Heinisch, Optimization of conditions in on-line comprehensive two-
593   dimensional reversed phase liquid chromatography. Experimental comparison with one-dimensional
594   reversed phase liquid chromatography for the separation of peptides J. Chromatogr. A 1421 (2015) 48–
595   59.
596   doi:10.1016/j.chroma.2015.08.052.
597

598   [3] A.F.G. Gargano, M. Duffin, P. Navarro, P.J. Schoenmakers, Reducing dilution and analysis time in
599   online comprehensive two-dimensional liquid chromatography by active modulation, Anal. Chem. 88
600   (2016) 1785–1793.
601   doi:10.1021/acs.analchem.5b04051.
602

603   [4] E. Sommella, O.H. Ismail, F. Pagano, G. Pepe, C. Ostacolo, G. Mazzoccanti, M. Russo, E. Novellino,
604   F. Gasparrini, P. Campiglia, Development of an improved online comprehensive hydrophilic interaction
605   chromatography × reversed-phase ultra-high-pressure liquid chromatography platform for complex
606   multiclass polyphenolic sample analysis, J. Sep. Sci. 40 (10) (2017) 2188–2197.
607   doi: 10.1002/jssc.201700134.
608

609   [5] D.R. Stoll, P.W. Carr, Two-dimensional liquid chromatography: A state of the art tutorial, Anal.
610   Chem. 89(1) (2017) 519–531.
611   https://doi.org/10.1021/acs.analchem.6b03506
612

613   [6] M. Muller, A.G.J. Tredoux, A. de Villiers, Predictive kinetic optimisation of hydrophilic interaction
614   chromatography × reversed phase liquid chromatography separations: Experimental verification and
615   application to phenolic analysis, J.of Chromatogr.A 1571 (2018) 107-120.
616   DOI: 10.1016/j.chroma.2018.08.004
617

618   [7] D.R. Stoll, H.R. Lhotka, D.C .Harmes, B. Madigan, J.J. Hsiao, G.O. Staples, High resolution two-
619   dimensional liquid chromatography coupled with mass spectrometry for robust and sensitive
620   characterization of therapeutic antibodies at the peptide level, J. of Chromatogr. B 1134-1135 (2019)
621   121832.
622   https://doi.org/10.1016/j.jchromb.2019.121832
623

624   [8] A.A. Alya, M. Muller, A. de Villiers, B.W.J. Pirok, T. Górecki, Parallel gradients in comprehensive
625   multidimensional liquid chromatography enhance utilization of the separation space and the degree of
626   orthogonality when the separation mechanisms are correlated, J. of Chromatogr. A 1628 (2020) 461452.
627   https://doi.org/10.1016/j.chroma.2020.461452
628

629   [9] S. Chapel, F. Rouvière, S. Heinisch, A theoretical and practical approach to manage high peak
630   capacity and low dilution in on-line comprehensive reversed-phase LC × reversed-phase LC: A
631   comparison with 1D-reversed-phase LC, LCGC Europe 33(5) (2020) 17–26.

632 [10] P. Dugo, F. Cacciola, T. Kumm, G. Dugo, L. Mondello, Comprehensive multidimensional liquid
633 chromatography: Theory and applications, J. Chromatogr. A 1184(1-2) (2008) 353–368.
634 doi: 10.1016/j.chroma.2007.06.074.

636 [11] G. Vanhoenacker, P. Sandra, K. Sandra, F. David, C. Brunelli, R. Szucs, M. Steenbeke, On-line
637 two-dimensional liquid chromatography (2D-LC) for the analysis of pharmaceuticals, LCGC Europe 29
638 (11) (2016) 610-617.

639 [12] K. J. Mayfield, R.A. Shalliker, H.J. Catchpoole, A.P. Sweeney, V. Wong, G.J. Guiochon, Viscous
640 fingering induced flow instability in multidimensional liquid chromatography, J. Chromatogr. A 1080
641 (2) (2005) 124–131.
642 doi:10.1016/j.chroma.2005.04.093.

644 [13] P. Jandera, T. Hájek, P. Česla, Effects of the gradient profile, sample volume and solvent on the
645 separation in very fast gradients, with special attention to the second-dimension gradient in
646 comprehensive two-dimensional liquid chromatography, J. Chromatogr. A. 1218 (2011) 1995–2006.
647 doi:10.1016/j.chroma.2010.10.095.

649 [14] J. De Vos, G. Desmet, S. Eeltink, A generic approach to post-column refocusing in liquid
650 chromatography, J. of Chromatogr. A 1360 (2014) 164-171.
651 doi: 10.1016/j.chroma.2014.07.072

653 [15] D.R. Stoll, R.W. Sajulga, B.N. Voigt, E.J. Larson, L.N. Jeong, S.C. Rutan, Simulation of elution
654 profiles in liquid chromatography − II: Investigation of injection volume overload under gradient elution
655 conditions applied to second dimension separations in two-dimensional liquid chromatography, J.
656 Chromatogr. A 1523 (2017) 162–172.
657 doi:10.1016/j.chroma.2017.07.041.

659 [16] R.J. Vonk, A.F.G. Gargano. E. Davydova, H.L. Dekker, S. Eeltink, L.J. de Koning, P.J.
660 Schoenmakers, Reducing dilution and analysis time in online comprehensive two-dimensional liquid
661 chromatography by active modulation, Anal. Chem. 87(10) (2015) 5387–5394.
662 doi: 10.1021/acs.analchem.5b00708.

664 [17] J. De Vos, G. Desmet, S. Eeltink, Enhancing detection sensitivity in gradient liquid chromatography
665 via post-column refocusing and strong-solvent remobilization, J Chromatogr A 1455 (2016) 86-92
666 doi: 10.1016/j.chroma.2016.05.046.

668 [18] S.S. Jakobsen, J.H. Christensen, S. Verdier, C.R. Mallet, N.J. Nielsen, Increasing flexibility in two-
669 dimensional liquid chromatography by pulsed elution of the first dimension: A proof of concept, Anal.
670 Chem. 89(17) (2017) 8723–8730.
671 doi:10.1021/acs.analchem.7b00758

673 [19] D.R. Stoll, K. Shoykhet, P. Petersson, S. Buckenmaier, Active Solvent Modulation: A valve-based
674 approach to improve separation compatibility in two-dimensional liquid chromatography, Anal. Chem.
675 89(17) (2017) 9260–9267.
676 https://doi.org/10.1021/acs.analchem.7b02046
677

678   [20] M. Pursch, A. Wegener, S. Buckenmaier, Evaluation of active solvent modulation to enhance two-
679   dimensional liquid chromatography for target analysis in polymeric matrices, J. of Chromatogr. A
680   1562 (2018) 78-86.
681   https://doi.org/10.1016/j.chroma.2018.05.059

682

683   [21] P. Yang, W. Gao, T. Zhang, M. Pursch, J. Luong, W. Sattler, A. Singh, S. Backer, Two-dimensional
684   liquid chromatography with active solvent modulation for studying monomer incorporation in
685   copolymer dispersants, J. of Sep. Sci. 42(17) (2019) 2805-2815.
686   https://doi.org/10.1002/jssc.201900283

687

688   [22] Y. Oda, N. Asakawa, T. Kajima, Y. Yoshida, T. Sato, On-line determination and resolution of
689   verapamil enantiomers by high-performance liquid chromatography with column switching, J. of
690   Chromatogr. 541 (1991) 411-418.
691   https://doi.org/10.1016/S0021-9673(01)96013-3

692

693   [23] E. Fornells, B. Barnett, M. Bailey, R.A. Shellie, E.F. Hilder, M.C. Breadmore, Membrane assisted
694   and temperature controlled on-line evaporative concentration for microfluidics, J. Chromatogr. A, 1486
695   (2017) 110-116.
696   https://doi.org/10.1016/j.chroma.2016.12.003

697

698   [24] M.E. Creese, M.J. Creese, J.P. Foley, H.J. Cortes, E.F. Hilder, R.A. Shellie, M.C. Breadmore,
699   Longitudinal on-column thermal modulation for comprehensive two-dimensional liquid
700   chromatography, Anal. Chem., 89 (2017) 1123-1130.
701   DOI: 10.1021/acs.analchem.6b03279

702

703   [25] B. Ji, B. Xia, J. Liu, Y. Gao, L. Ding, Y. Zhou, Application of fractionized sampling and stacking
704   for construction of an interface for online heart-cutting two-dimensional liquid chromatography, J.
705   Chromatogr. A, 1466 (2016) 199-204.
706   DOI: 10.1016/j.chroma.2016.09.014

707

708   [26] M. Enmark, D. Asberg, A. Shalliker, J. Samuelsson, T. Fornstedt, A closer study of peak distortions
709   in supercritical fluid chromatography as generated by the injection, J. Chromatogr. A 1400 (2015) 131–
710   139.
711   http://dx.doi.org/10.1016/j.chroma.2015.04.059

712

713   [27] L.N. Jeong, R. Sajulga, S.G. Forte, D.R. Stoll, S.C. Rutan, Simulation of elution profiles in liquid
714   chromatography—I: Gradient elution conditions, and with mismatched injection and mobile phase
715   solvents, J. Chromatogr. A. 1457 (2016) 41–49.
716   http://dx.doi.org/10.1016/j.chroma.2016.06.016.

717

718   [28] F. Gritti, M. Gilar, J. Hill, Mismatch between sample diluent and eluent: Maintaining integrity of
719   gradient peaks using in silico approaches, J. of Chromatogr. A 1608 (2019) 460414.
720   https://doi.org/10.1016/j.chroma.2019.460414

721

722   [29] S.R. Groskreutz, S.G. Weber, Temperature-assisted solute focusing with sequential trap/release
723   zones in isocratic and gradient capillary liquid chromatography: Simulation and experiment, J. of
724   Chromatogr. A 1474 (2016) 95-108.
725   https://doi.org/10.1016/j.chroma.2016.10.062

726 [30] L.N. Jeong, S.C. Rutan, Simulation of elution profiles in liquid chromatography – III. Stationary
727 phase gradients, J. of Chromatogr. A 1564 (2018) 128-136.
728 https://doi.org/10.1016/j.chroma.2018.06.007
729
730 [31] H. Poppe, J. Paanakker, M. Bronckhorst, Peak width in solvent-programmed chromatography : I.
731 General description of peak broadening in solvent-programmed elution, J. of Chromatogr. A 204 (1981)
732 77-84.
733 https://doi.org/10.1016/S0021-9673(00)81641-6
734
735 [32] L.N. Jeong, R. Sajulga, S.G. Forte, D.R. Stoll, S.C. Rutan, Simulation of elution profiles in liquid
736 chromatography—I: Gradient elution conditions, and with mismatched injection and mobile phase
737 solvents, J. of Chromatogr. 1457 (2016) 41-49.
738 https://doi.org/10.1016/j.chroma.2016.06.016
739
740 [33] R. Kaliszan, T. Bączek, A. Bucinski, B. Buszewski, M. Sztupecka, Prediction of gradient retention
741 from the linear solvent strength (LSS) model, quantitative structure-retention relationships (QSRR), and
742 artificial neural networks (ANN), J. of Sep. Sci. 26 (2003) 271–282.
743 https://doi.org/10.1002/jssc.200390033
744
745 [34] U.D. Neue, Nonlinear retention relationships in reversed-phase chromatography, Chromatogr. 63
746 (2006) S45-S53.
747
748 [35] S.L. Weatherbee, T. Brau, D.R. Stoll, S.C. Rutan, M.M. Collinson, Simulation of elution profiles
749 in liquid chromatography – IV: Experimental characterization and modeling of solute injection profiles
750 from a modulation valve used in two-dimensional liquid chromatography, J. of Chromatogr. A 1626
751 (2020) 461373.
752 https://doi.org/10.1016/j.chroma.2020.461373
753
754 [36] W.H. Press, S.A. Teukolsky, W.T. Vetterling, B.P. Flannery, Numerical Recipes: The art of
755 scientific computing (3rd ed.), Cambridge University Press, New York, USA, 2007, 1245 pp.
756
757 [37] F. Gritti, G. Guiochon, Separations by gradient elution: Why are steep gradient profiles distorted
758 and what is their impact on resolution in reversed-phase liquid chromatography, J. Chromatogr. A 1344
759 (2014) 66–75.
760 doi: 10.1016/j.chroma.2014.04.010
761
762 [38] A. Moussa, T. Lauer, D. Stoll, G. Desmet, K. Broeckhoven, Numerical and experimental
763 investigation of analyte breakthrough from sampling loops used for multi-dimensional liquid
764 chromatography, J. of Chromatogr. A 1626 (2020) 461283.
765 https://doi.org/10.1016/j.chroma.2020.461283
766
767
768
769

Figure Captions

771 **Figure 1.** Simulated mobile phase concentration (C_m) profiles plotted **(a)** as a function of time as
772 recorded at x=L and **(b-c)** as a function of the distance recorded at different subsequent times (resp. at t
773 = 0.018 min, 0.036 min, 0.051 min, 0.058 min, 0.064 min, 0.109 min, 0.245 min, 0.354 min, 0.409 min,
774 0.445 min for profiles 1-11). Each number i added to (a) represents the C_m-level recorded at the detector
775 line at the moment when profile i is observed in (b-c). **(d)** C_s-profiles corresponding to profiles nr. 1-6
776 in (b). **(e-f)** ϕ-profiles corresponding to the profiles 1-12 in (b-c). Dashed vertical line=detector line.
777 Simulation parameters: S_1=12.5, S_2=0.5, k_w=20, D_{ax}=3.86·10^{-8} m^2/s, u_0=0.0103 m/s, H=7.5 µm and
778 $V_{p,inj}$=15 µL. The stationary phase is only present between the x=0 and the x=0.03 m-point. Gradient
779 profile reaches head of column at t=0.14 min.

780 **Figure 2.** Conceptual drawing of migration process of sample solvent (bold line shape) and analyte
781 species band (stripe pattern) through column, showing **(a)** difference in migration speed between analyte
782 moving at $u=u_0/(1+k_s)$ and sample solvent band moving at $u=u_0$ and **(b)** dispersion process to explain
783 difference in retention behavior between species dispersing out of the injection solvent band at the
784 upstream (I) and the downstream flank of the band (see text for explanation). Double-headed arrows
785 represent dispersion process. Single-headed arrows represent u_0-velocity.

786 **Figure 3.** Simulated mobile phase concentration (C_m) profiles as a function of time as recorded at x=L
787 in response to a rectangular injection band ($V_{p,inj}$=25 µL) for **(a)** a series of analytes with different k_w-
788 value (k_w=10 (grey), 20 (blue), 50 (green), 100 (red)) and same S_1=10 and S_2=1, and **(b)** a series of
789 analytes with different S_1-value (S_1=5 (red), 7.5 (green), 10 (blue), 12.5 (orange), 15 (grey)) and same
790 k_w=20 and S_2=1. Other conditions same as in Fig. 1.

791 **Figure 4.** Zoom-ins on the effect of the axial dispersion of the analyte ($D_{ax,anal}$) and the solvent ($D_{ax,solv}$)
792 on the breakthrough-fraction and the retained peak fraction of the response profiles recorded as a
793 function of time at x=L (rectangular injection band with V_{inj}=15 µL). **(a)** constant $D_{ax,an}$= 3.86·10^{-8} m^2/s
794 and varying $D_{ax,solv}$=3.86·10^{-8} m^2/s (grey), 7.72·10^{-8} m^2/s (green), 1.16·10^{-7} m^2/s (blue), 1.54·10^{-7} m^2/s
795 (orange), 1.93·10^{-7} m^2/s (red). **(b)** constant $D_{ax,solv}$ = 3.86·10^{-8} m^2/s and varying $D_{ax,an}$ 3.86·10^{-8} m^2/s
796 (grey), 7.72·10^{-8} m^2/s (green), 1.16·10^{-7} m^2/s (blue), 1.54·10^{-7} m^2/s (orange), 1.93·10^{-7} m^2/s (red). **(c)**
797 case with $D_{ax,solv}$ = $D_{ax,an}$ =3.86·10^{-8} m^2/s (grey), 7.72·10^{-8} m^2/s (green), 1.16·10^{-7} m^2/s (blue), 1.54·10^{-7}
798 m^2/s (orange), 1.93·10^{-7} m^2/s (red). Other conditions: S_1=12.5, S_2=0.7, k_w=20, u_0=0.0103 m/s and H=7.5
799 µm.

800 **Figure 5. (a)** Rectangular injection bands with varying volume (V_{inj} = 1 µL(purple), 5 µL(grey), 10
801 µL(black), 12 µL(red), 15 µL(green), 25 µL(orange), 50 µL(blue)) leading to **(b)** a different mobile
802 phase concentration (C_m) profile recorded as a function of time at x=L. **(c)** Zoom-in at bottom-part of y-
803 axis of (b). **(d)** Zoom-in of (c) near the elution time of the retained peak fraction. Other conditions same
804 as in Fig. 1.

Figure 6. Simulated mobile phase concentration (C_m) profiles as a function of time as recorded at x=L in response to an injection band with **(a)** profiles with various degrees of tailing in space: α_2=0.01 (blue), α_2=0.05 (orange), α_1=0.10 (grey), α_1=0.15 (green), and **(b)** profiles with various degrees of fronting in space= α_2=0.01 (blue), α_2=0.03 (orange), α_1=0.07 (grey), α_1=0.15 (green). When one α was varied the other one was put on 0.01. Other conditions: S_1=12.5, S_2=0.7, k_w=15, V_{inj}=20 µL, u_0=0.0103 m/s and H=7.5 µm.

Figure 7. Experimental **(a)** and simulated **(b)** breakthrough profiles for caffeine for three different peak volumes (36 µL (red), 14 µL (green) and 0.7 µL (blue)). **(c,d)** zoom-in on lower part of y-axis of (a,b) respectively. Adopted retention parameters: k_w=11, S_1=24, S_2=2, u_0=0.0103 m/s and H=7.5 µm. Gradient conditions: 1-45% B in 0.54 min (normalized gradient slope s of 4%). Injection profile (see Fig. S-7a of the SM) with α_1=0.03, α_2=0.2, t_{dwell}=8.4 s and F_v=1.5 ml/min in Eq. (9).

Figure 8. Experimental **(a)** and simulated **(b)** breakthrough profiles for methylparaben for three different peak volumes (72 µL (red), 27 µL (green) and 25 µL (blue)). **(c,d)** zoom-in on lower part of y-axis of (a,b) respectively. Adopted retention parameters: k_w=23, S_1=13, S_2=0.7, u_0=0.0103 m/s and H=7.5 µm. Gradient conditions: 1-45% B in 0.54 min (normalized gradient slope s of 4%). Same injection profile as in Fig. 7.
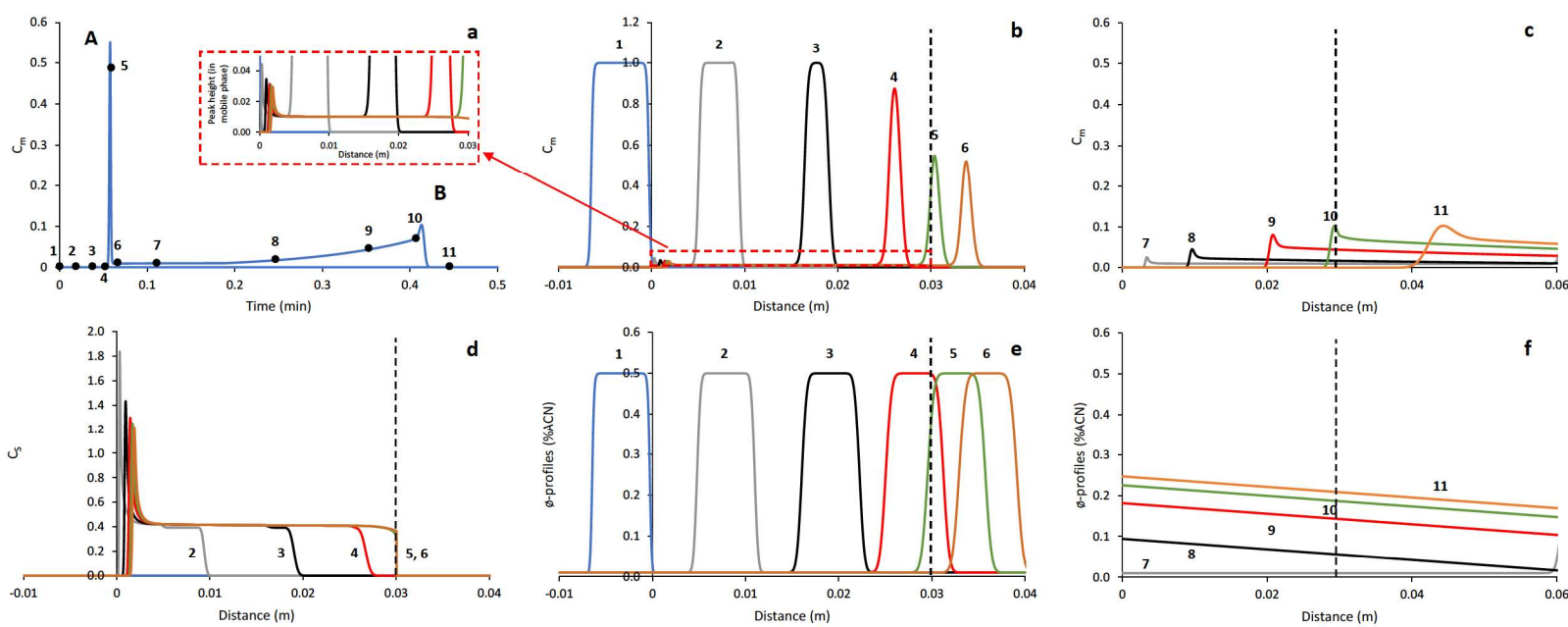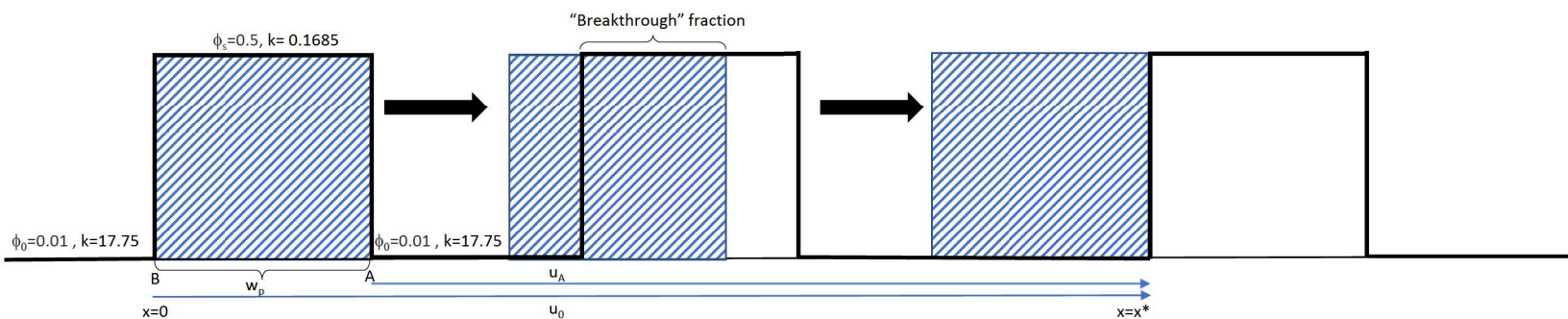
Fig 1: figure of how profiles are made
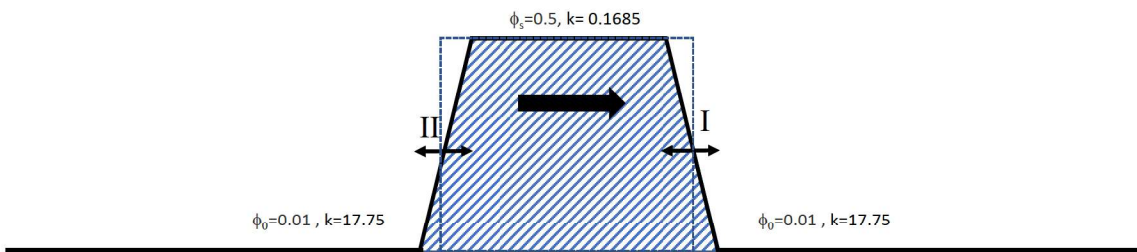
Fig 2: Process in column

a

$\phi_s=0.5$, k= 0.1685

"Breakthrough" fraction

$\phi_0=0.01$, k=17.75 $\phi_0=0.01$, k=17.75

B w_p A u_A

x=0 u_0 x=x*

b

$\phi_s=0.5$, k= 0.1685

II   I

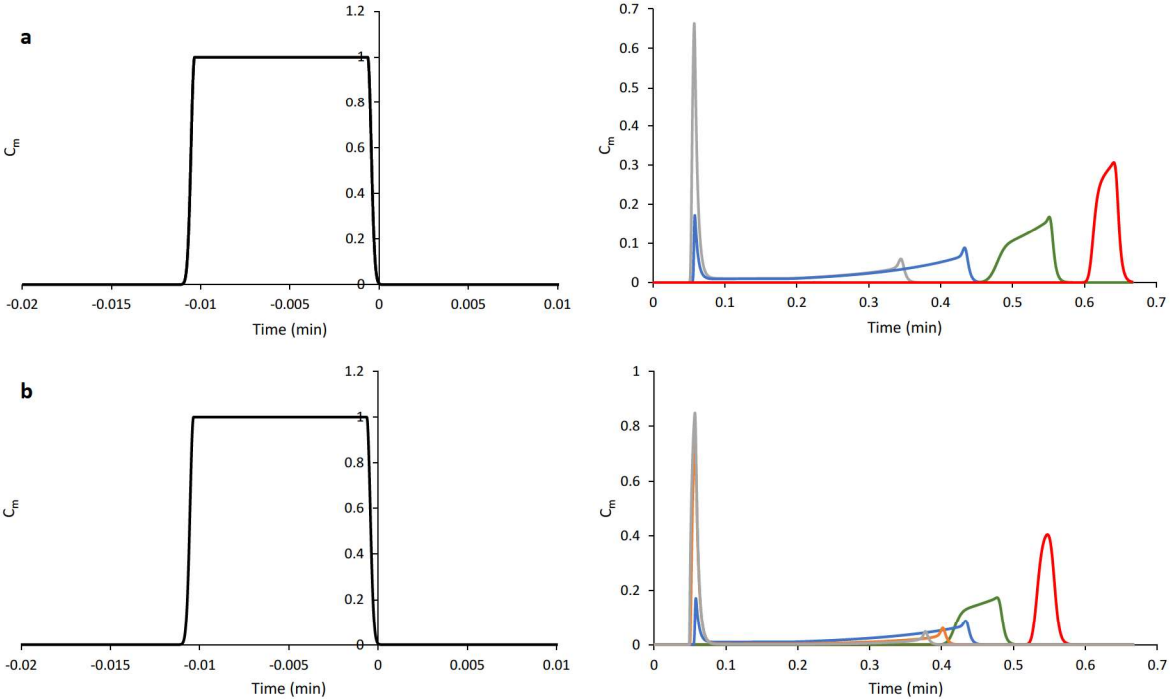$\phi_0=0.01$, k=17.75 $\phi_0=0.01$, k=17.75

Fig 3: a) Influence kw, b) Influence S1

Fig 4: a) Influence Dax
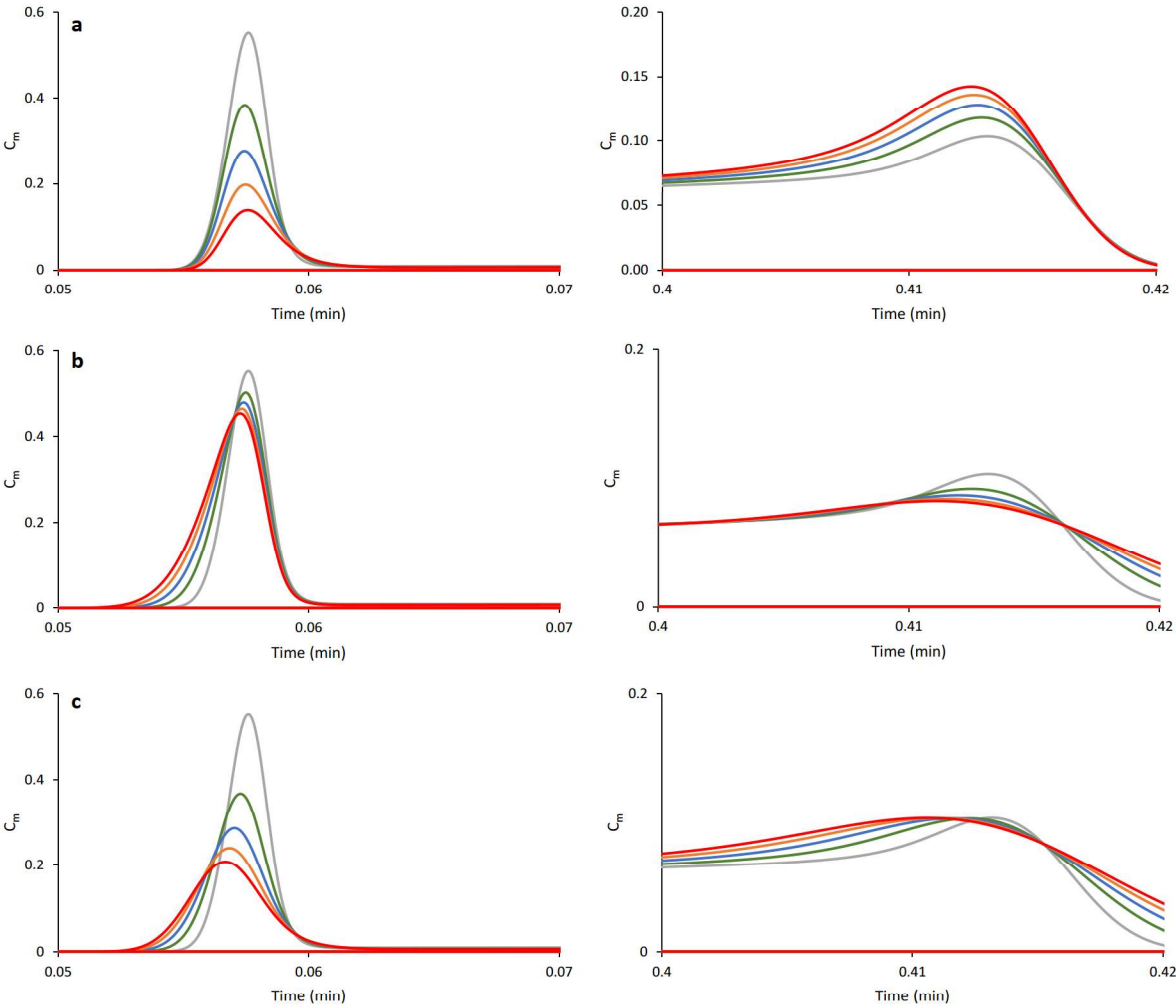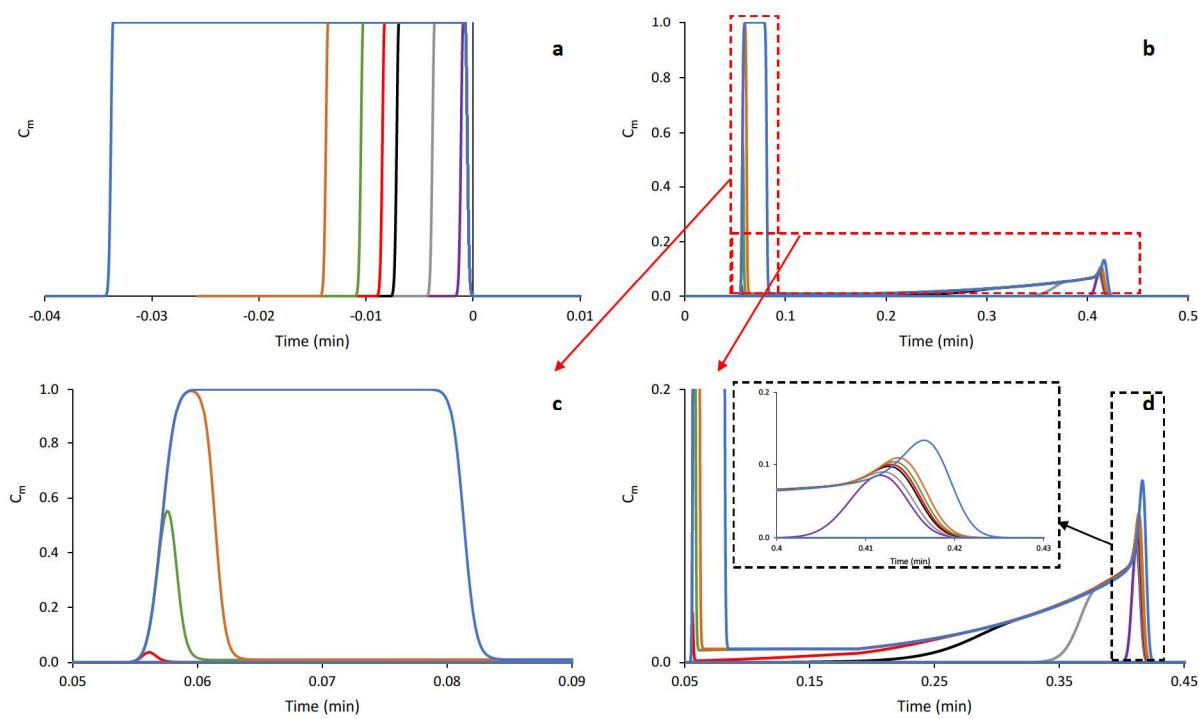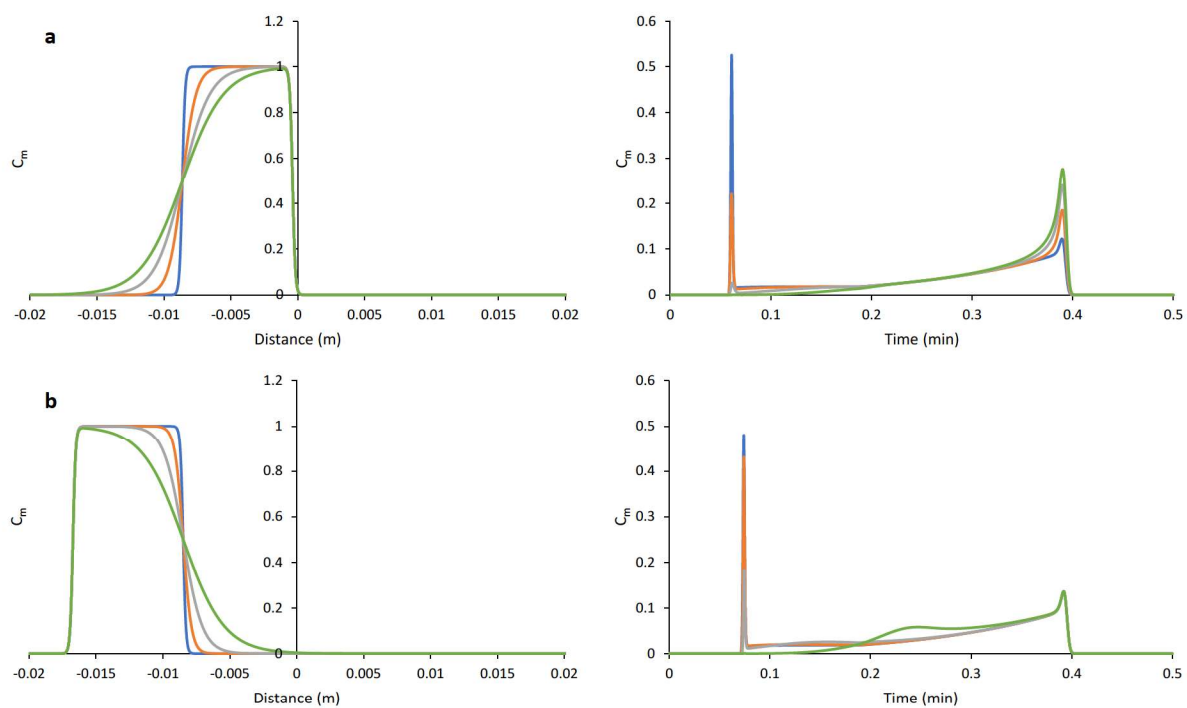
Fig 5: a) Influence injection volume

Fig 6: a) Influence tailing b) influence fronting

Fig 7 en 8 : Caffeine en Methylparaben